2008 IEEE International Conference on
Robotics and Automation
Pasadena, CA, USA, May 19-23, 2008

Optimum Design and Development of an XY Flexure Micromanipulator for Micro Scale Positioning

Yangmin Li, *Senior Member, IEEE,* and Qingsong Xu

***Abstract*— This paper presents the design and development procedures of a new decoupled XY micromanipulator for micro scale positioning applications. The manipulator is featured with parallel-kinematic architecture, flexure hinge-based joints, and piezoelectric actuation. Based on the lumped model, the efficient models for kinematics, statics and dynamics of the XY stage have been obtained, which are verified by resorting to the finite element analysis via ANSYS software package. Moreover, the stage dimensions are optimized through the particle swarm optimization (PSO) approach, and a manipulator with performances satisfying the requirements is generated. Furthermore, a prototype of the manipulator has been fabricated via the wire-EDM process. The developed micromanipulator is expected to be adopted in practical applications.**

***Index Terms*— Micro-positioning stages; Parallel robots; Flexure mechanisms; Optimal design.**

I. Introduction

As the increasing activities around the research and development in micro and nano scales technology, micromanipulators with ultrahigh precision play more and more important roles in such applications as bio-cell manipulation, optical fibers alignment, micro component assembly, and scanning probe microscopy, etc. In order to suit above situations, the manipulators are preferred to be designed with high resolution, high repeatability, and high bandwidth capabilities, while the manipulators themselves may be in macro scale with the size of tens or hundreds of millimeters instead.

The design of a proper manipulator satisfying all of the requirements is a challenging systemic work since it needs the integrated consideration of all issues including mechanical joints, actuators, sensors, materials, fabrication, kinematic schemes, control schemes, and so on. In recent works relating to the design and development of micromanipulators for micro- or nano-positioning, a precision $XY\theta$ stage featuring flexural element, electromagnetic actuation, and capacitance sensing was presented in [1]. A small-scale nanopositioner named μHexFlex with six-axis was proposed to employ a parallel compliant mechanism actuated with three two-axis thermo-mechanical micro-actuators [2]. In addition, the design of a large-displacement decoupled XYZ flexure parallel mechanism was elaborated in [3], where the mechanism was constructed with notch hinge-based flexure joints and fabricated by aluminum alloy. Besides, the design, fabrication and control of a piezo-driven, parallel-kinematic flexure XY stage was described in [4], which reported on a relative comprehensive work since it covered the major issues of joints, actuators, sensors, kinematic scheme, and controller design, etc. In addition, although some commercial micro-positioning products can be found from companies such as PI, Thorlabs, etc., theoretical analysis and design diversity will still be necessary in the academic field since it will push forward the development and maturity of current industrial products. In this paper, we are concentrated on a thorough description of the entire analysis process including the design, modeling, optimization, and fabrication of a new precision XY micromanipulator with sub-micron resolution. A parallel mechanism usually owns a greater stiffness and lower inertia than a serial one, it enables the generation of higher bandwidth of the servomechanism. Besides, flexure hinges have dominant superiority over traditional joints in precision manipulation since flexure hinges endow a mechanism with such merits as no clearance and backlash, no friction and lubrication, and vacuum compatibility, which will contribute to an ultrahigh accuracy. Furthermore, the piezoelectric actuator (PZT) is preferred in such situations as greater actuation force, higher stiffness, and faster response characteristics are required.

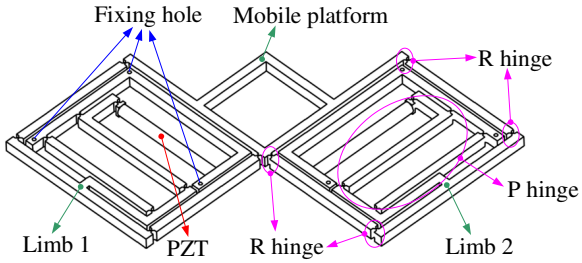

Fig. 1. The designed XY CPM.

The stage in the current research is designed based on a parallel kinematic mechanism (PKM) composing of flexure hinge-based joints, which is driven by two piezoelectric actuators (PZTs). Concerning the fabrication aspect, the monolithic stage is manufactured from a piece of Al 7075 alloy by the wire-EDM (electrical discharge machining) process. Whereas before the development of the micromanipulator, the architecture parameters for the stage need to be optimized with respect to desired performances. Hence,

This work was supported by the research committee of University of Macau under Grant RG065/06-07S/LYM/FST and Macao Science and Technology Development Fund under Grant 069/2005/A.

The authors are with the Department of Electromechanical Engineering, Faculty of Science and Technology, University of Macau, Av. Padre Tomás Pereira S.J., Taipa, Macao SAR, P. R. China ymli@umac.mo

in order to characterize the properties of the manipulator for the optimization purpose, mathematical models capable of representing kinematics, statics, and dynamics of the stage are indispensable for an efficient architecture optimization process without intensive computation.

II. Architecture Description of an XY CPM

A micromanipulator featuring parallel mechanism and flexure hinges is referred as a compliant parallel micromanipulator (CPM) throughout this paper. The designed XY CPM stage is illustrated in Fig. 1. It employs flexure hinges at all joints, and consists of a mobile platform and two limbs with identical kinematic structure. Each limb consists of a parallelogram including four flexure revolute (R) hinges or two R-R legs, and a flexure prismatic (P) hinge (Fig. 2) in sequence. The P joint within each limb is fixed at the base via three fixing screws and actuated by a PZT.

The main problems concerning flexure hinge are the center-shift and stress concentration phenomena [5], [6], which lead to a degraded accuracy and fatigue risk of the CPM, respectively. In consequence, the hinge with right-circular shape is adopted since it possesses the smallest center-shift compared to other types of hinges, and the materials with higher ratio of yield strength to Young's modulus (such as Ti alloy, Al alloy, stainless steal, etc.) are selected to build the stage. Additionally, although PZTs bear some disadvantages including limited output displacement, hysteresis and nonlinearity, etc., they can be improved by utilizing lever amplification mechanism and adding displacement sensors in the actuators or the CPM end-effectors, respectively. An initial version of the designed CPM was previously proposed by the authors in [7]. In this paper, the stage structure has been significantly improved as shown in Fig. 1, which is expected to overcome the drawbacks and find its application in planar micro/nano scale positioning. If an XYZ motion is needed, the designed XY stage can be placed on a one-DOF translational stage in vertical direction to meet the requirement.

In the design stage for the XY CPM, the main objective is to establish simple yet accurate enough models to assess the CPM performances without intensive computation as in FEA. Here, the lumped model based on the pseudo-rigid-body (PRB) concept [8] is utilized to evaluate the design of CPM. It means that all of the flexure hinges can be replaced by a revolute joint combined with a torsional spring, whereas other elements can be considered as rigid bodies.

III. Kinematics and Parasitic Motion Analyses

In order to elaborate the working principle of the XY CPM, we assume that limb 1 is driven by the PZT with a displacement q_1 whereas the limb 2 remains un-driven. Under such case, the input q_1 will be amplified by the lever in the P joint, which produces a displacement d_1 as shown in Fig. 2(b). Then, the displacement d_1 is transmitted to the mobile platform through the two parallel R-R legs in limb 1. The pure translation of the mobile platform along the x-axis will be guaranteed by the two R-R legs composing a

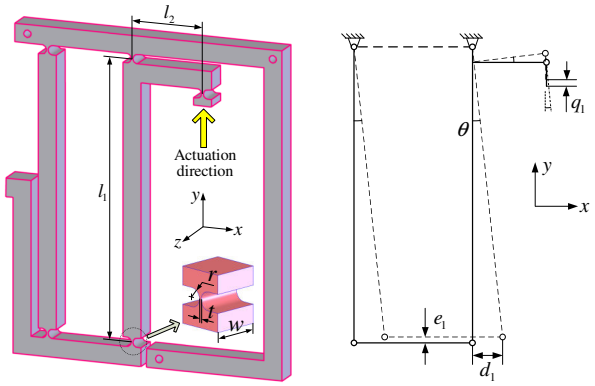

(a) (b)

Fig. 2. Parameters representation of the actuation P joint.

parallelogram in limb 2. Due to a symmetry of the CPM, the input displacement q_2 will be amplified as d_2 and then transferred to the mobile along the y direction accordingly.

A. Property of the Amplification P Joint

To illustrate the properties of the adopted P joint, the kinematics and stiffness will be analyzed below.

With reference to Fig. 2, the theoretical amplification ratio of the lever can be expressed as:

$$A_P = l_1/l_2. \tag{1}$$

By using the amplification mechanism, the stroke of the actuator can be magnified by a factor of A_P, whereas the resolution of the actuator will be reduced by A_P times as the expense. Therefore, a tradeoff is needed in the design of the amplification P joint.

The actuation stiffness describing the relationship between the input force and the corresponding displacement of the prismatic joint can be calculated as follows. Let the force and displacement created by the PZT be F and q_1, respectively, which are applied on the amplification flexure P joint. Then, the theoretical output displacement of the P joint can be expressed as:

$$d_1 = A_P\, q_1. \tag{2}$$

In addition, assign the same dimensions to the five notch hinges of the P joint, then the hinges' rotation angle around the z-axis (Fig. 2) equal the same value, namely, θ. Hence, the potential energy of the P joint due to elastic deflections can be expressed as:

$$P_p = \frac{1}{2}K_P q_1^2 = 5 \times \frac{1}{2}k\theta^2, \tag{3}$$

where

$$k = \frac{2Ewt^{2.5}}{9\pi r^{0.5}} \tag{4}$$

is the rotation stiffness of the right circle flexure hinge around the z-axis [9], and the relationship between the small rotation angle θ and the displacement q_1 can be written as:

$$q_1 = l_2\theta. \tag{5}$$

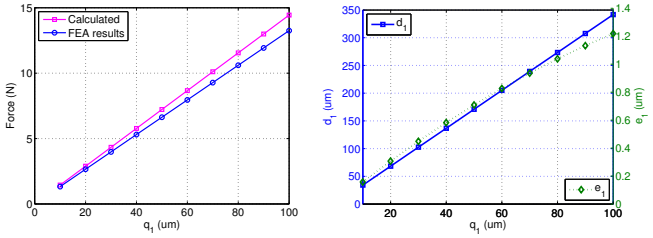

(a) Force-deflection relationship. (b) Output versus input motion.

Fig. 3. FEA results of the actuation P joint.

TABLE I
MAIN PARAMETERS OF AN XY CPM

Architectural parameters (mm)					
a	l_1	l_2	r	t	w
152.0	152.0	38.0	2.5	1.0	12.7
Material parameters					
Young's modulus		Yield strength	Poisson's ratio	Density	
71.7 GPa		503 MPa	0.33	2.81×10^3 kg/m^3	

Substituting (2), (4), and (5) into (3) allows the calculation of the stiffness of the amplification P joint in the actuation direction:

$$K_P = \frac{10A_P^2 Ewt^{2.5}}{9\pi r^{0.5} l_2^2}. \tag{6}$$

For an amplification P joint with parameters elaborated in Table I, the nonlinear statics FEA is performed with ANSYS, and the force-deflection relationship is plotted in Fig. 3(a). It can be observed that the simulated and calculated stiffness values are very close, which validates the accuracy of the stiffness model in (6). Moreover, the linear plot reveals the absence of stress stiffening in the P joint.

In addition, the relationships between the input and output displacements are shown in Fig. 3(b), which exhibits that the amplification ratio of the flexure P joint is about 3.42 being less than the theoretical value $A_P = 4$. The lost motion comes from the reason that the elements other than notch hinges are not fully rigid bodies. Besides, the actuation P joint introduces a parasitic translational motion vertical to its working direction. In what follows, a decoupled XY CPM design is attempted by compensating for the aforementioned parasitic motion.

B. Parasitic Motion Analysis of the XY CPM

The key technique to design a decoupled XY CPM is to eliminate its parasitic motion or cross-talk of the two axes. Under the situation that limb 1 of the CPM is driven by a PZT, the parasitic motions induced by limbs 1 and 2 are represented in Figs. 2(b) and 4(b), respectively, which can be expressed as follows.

$$e_1 = l_1\big[1-\cos(\theta)\big], \tag{7}$$
$$e_2 = a\big[1-\cos(\beta)\big], \tag{8}$$

where

$$\theta = \sin^{-1}(d_1/l_1) \approx d_1/l_1, \tag{9}$$
$$\beta = \sin^{-1}(d_1/a) \approx d_1/a. \tag{10}$$

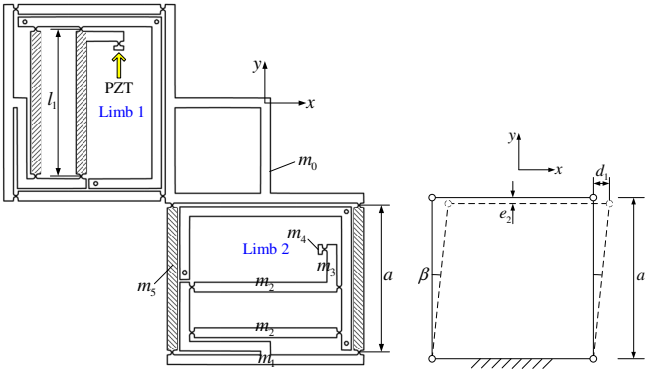

(a) (b)

Fig. 4. Parasitic motion representation of the XY CPM.

Taking into account the directions of the parasitic motions, one can see that e_1 is along the $+y$ axis, while e_2 is along the $-y$ direction instead. In accordance with the relationship between e_1 and e_2, three cases may occur. For the sake of eliminating the parasitic motions in the y direction, the case of $e_1 = e_2$ should be adopted. In view of (7) and (8), we can deduce that it is the situation of

$$l_1 = a. \tag{11}$$

Due to the symmetric structure of the CPM, it is observed that if the CPM is designed with the parameters satisfying (11), the output translational motion is decoupled. Then, we have

$$d_1 = x, \quad d_2 = y, \tag{12}$$
$$\dot{d}_1 = \dot{x}, \quad \dot{d}_2 = \dot{y}. \tag{13}$$

A more detailed relation between the parasitic motion of the mobile platform and the parasitic motions caused by the two limbs will be established by a nonlinear modeling for the entire CPM, which is planned in the next step work of the research.

Another factor that may cause parasitic motions of the stage is the adopted flexure hinges themselves. Although the employed right-circular notch hinge has better accuracy than the hinge with other types of notch shape, the shift of rotation center and the compliances in other working directions still exist. Referring to the flexure hinge indicated in Fig. 2, we can see that the rotation around the z axis (with stiffness $K_{\theta_z - M_z}$) is its working direction. However, the hinges within legs also bear loads along the y axis (with stiffness $K_{u_y - F_y}$) and forces along the x axis (with stiffness $K_{u_x - F_x}$) directions during the operation. In order to make the flexure hinge more sensitive to the rotation about the working direction and more unsensitive to the passive directions, the following two stiffness ratios should be made as small as possible:

$$\varepsilon_1 = \frac{K_{\theta_z - M_z}}{K_{u_y - F_y}} \quad \text{and} \quad \varepsilon_2 = \frac{K_{\theta_z - M_z}}{K_{u_x - F_x}}. \tag{14}$$

Based upon the approximate stiffness equations presented in [9], the two stiffness ratios can be expanded in terms of

the hinge parameters:

$$\varepsilon_1 = \frac{2t^{2.5}}{9\pi r^{0.5}}\left[\pi\left(\frac{r}{t}\right)^{0.5} - 2.57\right] \quad \text{and} \quad \varepsilon_2 = r^2. \quad (15)$$

The above equations are valid in the ranges of

$$0 < \frac{t}{2r} \leq 0.2 \quad (16)$$

so as to keep the deviations with respect to the exact models within 10% [10]. Other performances of the XY CPM are studied in details in the following discussions.

IV. Statics and Dynamics Evaluation

The statics analysis of the CPM is helpful for the selection of actuators with sufficient output force to drive the CPM.

A. Statics Analysis

1) Static Forces Generation: Under the assumption of absence of external forces, the forces created by PZTs should be equivalent to the internal elastic forces due to the flexure hinges at the statics state. In what follows, we assume that limb 1 of the CPM is actuated by a PZT with a force F_1 and the corresponding input displacement is q_1, while the PZT inscribed in limb 2 remains un-driven.

Concerning with limb 1, the deformation mainly comes from the five hinges of the actuation P joint as shown in Fig. 2. Hence, the actuation force (F_{11}) contributing to the counteraction of the internal force in limb 1 can be calculated by considering (6), i.e.,

$$F_{11} = K_P\, q_1. \quad (17)$$

The output displacement ($d_1 = A_P\, q_1$) of the actuation P joint in limb 1 causes a displacement (d_1) to the CPM mobile platform along the x direction, and the same displacement to limb 2 in x direction as depicted in Fig. 4. The displacement (d_1) will cause the four hinges constructing the parallelogram of limb 2 to rotate with the same angle (β). Likewise, the stiffness of limb 2 in the x direction can be calculated as:

$$K_2 = \frac{8Ewt^{2.5}}{9\pi r^{0.5}a^2}. \quad (18)$$

Then, the partial actuation force (F_{12}) used to compensate for the internal force in limb 2 is

$$F_{12} = K_2\, A_P\, q_1. \quad (19)$$

Consequently, the actuation force F_1 inducing a displacement d_1 of the CPM can be calculated as the summation of F_{11} and F_{12}. It follows that the actuation stiffness of the XY CPM, i.e., the relationship between the actuation force and the corresponding displacement related to the P joint, can be determined by

$$K_q = \frac{F_1}{q_1} = K_P + K_2\, A_P = \frac{Ewt^{2.5}(10A_P^2 + 8A_P)}{9\pi r^{0.5}a^2}. \quad (20)$$

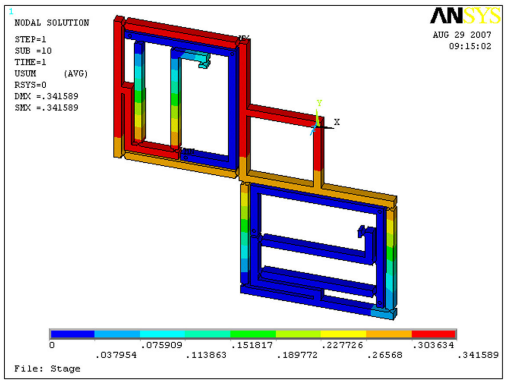

Fig. 5. Finite element model of the XY stage.

2) Statics Validation with FEA: Considering the XY CPM with parameters described in Table I, assume that the input displacement $d_1 = 100\,\mu$m is applied on the actuation P joint within limb 1. The actuation force can be computed as $F_{cal} = 17.33$ N, and the stiffness K_q can be calculated as $K_q^{cal} = 173.3$ N/mm. Moreover, the FEA is performed with ANSYS to validate the derived statics equation. In the simulation, the 20-node element SOLID186 is adopted to mesh the model, and the input displacements are assigned on the first actuation P joint. The deformed shape of the CPM is shown in Fig. 5, and the actuation force is determined as $F_{sim} = 20.37$ N. Furthermore, the actuation stiffness $K_q^{sim} = 203.7$ N/mm can be obtained from the simulation results.

It can be observed that there is a difference between the calculated actuation stiffness K_q^{cal} and the simulated one K_q^{sim}. The derivation of the calculated value with respect to the simulation result is 14.9%.

B. Dynamics Analysis

1) Dynamics Modeling of the CPM: Due to the merits of neglecting the consideration for the constraint forces, the Lagrange's motion equations are adopted for the dynamics modeling of the XY CPM. In order to obtain the dynamic model, the variables $\mathbf{q} = [q_1 \;\; q_2]^T$ are chosen as the generalized coordinates. Then, both potential and kinetic energies of the CPM should be expressed in terms of the selected coordinates and their derivatives. We assume that the potential energies come from the elastic deformations of the CPM.

By expressing the elastic potential and kinetic energies of the actuation P joints, R-R legs, and mobile platform, respectively, the energy function L for the entire CPM can be generated finally. The Lagrangian motion equations can be derived based on the generalized coordinates $\mathbf{q}$ according to:

$$\frac{d}{dt}\cdot\frac{\partial L}{\partial \dot{q}_i} - \frac{\partial L}{\partial q_i} = F_i, \quad i = 1,\, 2,\, 3, \quad (21)$$

where q_i denotes the i-th generalized coordinate and F_i is the i-th actuation force. Substituting (12) and (13) into (21),

allows the generation of dynamic equations

$$\mathbf{M}\ddot{\mathbf{q}} + \mathbf{K}\mathbf{q} = \mathbf{F}, \tag{22}$$

where $\mathbf{M} = \text{diag}\{M\}$ is the mass matrix, $\mathbf{K} = \text{diag}\{K\}$ is the stiffness matrix, and $\mathbf{F} = [F_1 \;\; F_2]^T$ denote the vectors for the actuation forces, respectively, with the following notations:

$$M = 16m_0 + 16m_1 + \frac{32}{3}m_2 + \frac{1}{3}m_3 + m_4 + \frac{128}{3}m_5, \tag{23}$$

$$K = \frac{288Ewt^{2.5}}{9\pi r^{0.5}a^2}, \tag{24}$$

where m_0 is the mass of the mobile platform, and the masses m_1 to m_5 are indicated in Fig. 4.

2) Modal Analysis and Simulation Validations: In general, the modal analysis can be accomplished by the FEA software package such as ANSYS. However, it requires intensive computation to perform a full-scale FEA in the optimization of the CPM. Thus, an analytical modal analysis is necessary for the design of a CPM with specified natural frequency. Commonly, to avoid exciting the structural oscillation and resonance of the CPM system, the natural frequency of the mechanism (f_{mech}) in a servo control system should be no less than two times higher than the frequency of the driving system (f_{ctrl}). It follows that a higher natural frequency of the mechanism allows a higher control frequency of the driving system. Based on the theory of vibrations, the dynamic equation of undamped free vibration of the CPM system can be expressed as:

$$\mathbf{M}\ddot{\mathbf{q}} + \mathbf{K}\mathbf{q} = \mathbf{0}, \tag{25}$$

which allows the calculation of the natural frequency, i.e., $f = \frac{1}{2\pi}\sqrt{K/M}$ Hertz.

As a case study, with the kinematic and physical parameters described in Table I, the natural frequency of the XY stage can be calculated as f_{mech} =27.57 Hz. Moreover, the modal analysis of the CPM is performed with ANSYS software. The simulation results exhibit that the first two vibration shapes are translations along the two axes of the frame. Due to a symmetric structure of the CPM, the first two natural frequencies are almost the same. Besides, it can be seen that the first one (23.83 Hz) obtained by ANSYS agrees approximately with the calculated value from the dynamic model with a deviation of 15.7%.

V. Dimension Optimization

A review of the above analyses reveals that the performances of the CPM in terms of kinematics, statics and dynamics are all dependent on its architectural parameters. Consequently, in order to develop a CPM for practical application, it is a key step to determine its dimensions by taking into account its performances such as parasitic motion, stiffness value, and natural frequency, etc., simultaneously. In this study, the true values for the CPM stiffness and natural frequency are taken to be those generated from the FEA. Considering that the differences between calculated and simulated results for the stiffness and natural frequency are within about $\pm 15\%$, a compensation factor $\eta = 0.85$ is adopted in the optimization process to correct the derived analytical models.

TABLE II
Optimized Dimensions for the XY Stage

Parameter	a	l_1	t	r	w
Value (mm)	152.15	152.15	1.03	2.54	12.98

A. Objective Function

With the goal of enhancing the accuracy property of the CPM, the main objective of the dimension optimization is to obtain a CPM with minimum parasitic motions subject to other performance constraints, and the optimal design problem can be stated as follows:

- Variables to be optimized: a, l_1, t, r and w.
- Minimize: Parasitic motions (ε_1, ε_2)
- Subject to:
  1) Actuation stiffness value $K_q/\eta \leq K_{PZT}$
  2) Natural frequency $2f_{ctrl} \leq f_{mech}\eta \leq f_{max}/15$
  3) Elimination of parasitic motion guaranteed by (11)
  4) Accuracy valid range ensured by (16)
  5) Parameter ranges: $60\,\text{mm} \leq a \leq 160\,\text{mm}$, $60\,\text{mm} \leq l_1 \leq 160\,\text{mm}$, $0.3\,\text{mm} \leq t \leq 2\,\text{mm}$, $2\,\text{mm} \leq r \leq 6\,\text{mm}$, and $8\,\text{mm} \leq w \leq 16\,\text{mm}$

So, five parameters ($\mathbf{n} = [a, l_1, t, r, w]^T$) need to be optimized. The objective function for minimization is taken as:

$$f(\mathbf{n}) = \varepsilon_1 + \varepsilon_2 = \frac{2t^{2.5}}{9\pi r^{0.5}}\left[\pi\left(\frac{r}{t}\right)^{0.5} - 2.57\right] + r^2. \tag{26}$$

As far as the constraint conditions are concerned, the actuation stiffness of the CPM should not exceed the stiffness of the adopted PZT, i.e., $K_{PZT} = 1000\,\text{N/mm}$. The natural frequency should be no less than two times of the frequency of the servo system which is taken as $f_{ctrl} = 12\,\text{Hz}$ in this case and be no greater than one fifteenth of the maximum sampling rate $f_{max} = 500\,\text{Hz}$ of the numerical control so as to avoid exciting resonance of the system. Besides that, since the CPM will be manufactured by the wire-EDM process, the width of the thinnest portion of the notch hinge should be no less than 0.3 mm corresponding to the maximum tolerance of ± 0.01 mm. The minimum value of the distance l_1 is restricted by the length of the adopted PZT (132 mm) with the addition of proper assembly spaces, and the upper bounds for design variables are all limited so as to generate a compact manipulator.

B. Optimization Results and Performance Validation

The particle swarm optimization (PSO) is adopted in this research work although other methods can also be employed. Compared to the genetic algorithm (GA), the PSO has no evolutionary operators such as crossover and mutation. Thus, the advantages for PSO are the ease to implement and few parameters to adjust.

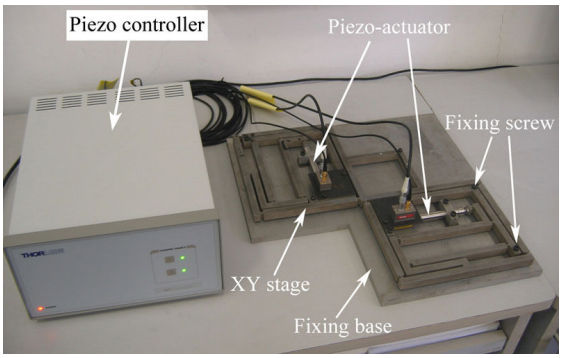

Fig. 6. Photograph of the XY CPM prototype.

In the current five-dimensional optimization problem, the population size is set as 40, the local and global acceleration constants are all assigned as 2.0, and then the swarm is manipulated by the operating equations [11]. Additionally, three options are set as the termination criteria. One is the maximum number of iterations (3000) for the optimization procedure, another is the minimum global error gradient (1.0E−6) which is the error between two neighboring particles with the best fitness values, and the third criterion is the maximum number of iterations without error change, that is chosen as 500.

The optimization is implemented with MATLAB, where the procedure is initialized with random start values within search spaces, and a total of 20 independent runs are carried out on a personal computer. Although the PSO has the stochastic property, i.e., it makes random choices, each run converges to the same value for the objective function due to the reason that the selected termination criteria are sufficient. The optimized CPM dimensions are described in Table II.

Moreover, the FEA has been carried out via ANSYS for the stage. The simulation results show that the manipulator possesses an actuation stiffness of 173.3 N/mm and a natural frequency of 23.8 Hz, which all satisfy the assigned performance demands. Besides, the manipulator has a maximum cross-talk of 3.1% between the two working axes. The natural frequency will be improved by reducing the overall size of the manipulator, and the parasitic motions will be further reduced by making use of a nonlinear modeling of the stage.

VI. Prototype Development and Future Works

For the convenience of manufacture, the CPM parameters as elaborated in Table I (approximate to those in Table II) are adopted to develop the CPM prototype, which is graphically shown in Fig. 6. The stage is fabricated with a kind of light material called Al 7075 alloy. To make a tradeoff between the stroke and resolution of the PZT, one type of PZT, namely, PAZ015 produced by Thorlabs, Inc. is adopted to drive the XY stage. The PZT actuator possesses a stroke of $Q = 100\,\mu$m, an open-loop resolution of 100 nm, and 25 nm closed-loop resolution with strain gage sensory feedback. In addition, the embedded strain gage displacement sensor can eliminate the hysteresis property and allow a liner output of the PZT. The FEA results show that the CPM can provide a workspace range of $315\times315\,\mu\text{m}^2$ with a closed-loop resolution of 78 nm. Additionally, the two-axis controller BPC002 from the Thorlabs is used to drive the PZT with a voltage range from 0 to 75 V.

Moreover, the overall size of the CPM will be reduced in the next step work by adopting a smaller PZT, and the relatively large cross-talk value will be compensated by employing a displacement feedback controller.

VII. Conclusion

This paper is focused on the design and development issues for a new precision XY micromanipulator, which possesses a relatively simple structure. Based on the PRB simplification model, the kinematics and parasitic motion of the manipulator have been analyzed in details, and the statics is solved and validated through the FEA via ANSYS. In addition, the dynamics model has been established by the Lagrangian approach and the modal analysis is implemented, which is also verified by the FEA. Moreover, the optimum design for the CPM parameters has been carried out by PSO method. The performances of the optimized CPM are predicted by the FEA simulations. Besides, a prototype of the resulted CPM has been developed using the hardware available, and the fabricated CPM is expected to be adopted in the application of micropositioning of objects in micro scale.

References

[1] K.-S. Chen, D. Trumper, and S. Smith, "Design and control for an electromagnetically driven X-Y-θ stage," *Precis. Eng.*, vol. 26, no. 4, pp. 355–369, 2002.

[2] S.-C. Chen and M. L. Culpepper, "Design of a six-axis micro-scale nanopositioner—μhexflex," *Precis. Eng.*, vol. 30, pp. 314–324, 2006.

[3] X. Tang, I.-M. Chen, and Q. Li, "Design and nonlinear modeling of a large-displacement XYZ flexure parallel mechanism with decoupled kinematic structure," *Rev. Sci. Instrum.*, vol. 77, p. 115101, 2006.

[4] Q. Yao, J. Dong, and P. Ferreira, "Design, analysis, fabrication and testing of a parallel-kinematic micropositioning XY stage," *Int. J. Mach. Tools Manuf.*, vol. 47, no. 6, pp. 946–961, 2007.

[5] N. Lobontiu, J. S. N. Paine, E. Garcia, and M. Goldfarb, "Design of symmetric conic-section flexure hinges based on closed-form compliance equations," *Mech. Mach. Theory*, vol. 37, no. 5, pp. 477–498, 2002.

[6] T.-F. Niaritsiry, N. Fazenda, and R. Clavel, "Study of the sources of inaccuracy of a 3DOF flexure hinge-based parallel manipulator," in *Proc. of IEEE Int. Conf. on Robotics and Automation*, 2004, pp. 4091–4096.

[7] Y. Li and Q. Xu, "A novel design and analysis of a 2-DOF compliant parallel micromanipulator for nanomanipulation," *IEEE Trans. Automat. Sci. Eng.*, vol. 3, no. 3, pp. 248–254, 2006.

[8] L. L. Howell, *Compliant Mechanisms*. New York: Wiley, 2001.

[9] J. Paros and L. Weisbord, "How to design flexure hinges," *Machine Design*, vol. 37, pp. 151–156, 1965.

[10] S. T. Smith, *Flexures: Elements of Elastic Mechanisms*. CRC Press, 2000.

[11] M. Clerc and J. Kennedy, "The particle swarm-explosion, stability, and convergence in a multidimensional complex space," *IEEE Trans. Evol. Comput.*, vol. 6, no. 1, pp. 58–73, 2002.